Applied Energy 130 (2014) 280–288

Contents lists available at ScienceDirect

Applied Energy

journal homepage: www.elsevier.com/locate/apenergy

Numerical assessment of the thermodynamic performance of thermoelectric cells via two-dimensional modelling ☆

Klaudio S.M. Oliveira, Rodrigo P. Cardoso, Christian J.L. Hermes *

Laboratory of Thermodynamics and Thermophysics, Federal University of Paraná, 81531990 Curitiba, PR, Brazil

HIGHLIGHTS

- A 2-D model for thermoelectric cells is advanced based on the finite-volume method.
- The model accounts for the Fourier, the Thomson, and the Joule effects.
- The model predictions were validated against experimental data.
- The effects of the thermoelectric properties and the cell geometry were assessed.

ARTICLE INFO

Article history:
Received 12 March 2014
Received in revised form 20 May 2014
Accepted 21 May 2014
Available online 13 June 2014

Keywords:
Thermoelectric cooling
Two-dimensional model
Sensitivity analysis
Finite-volume method

ABSTRACT

The present paper is aimed at putting forward a two-dimensional model for thermoelectric cells. The energy conservation equation was formulated in order to account for the Fourier (heat) conduction, the Thomson (thermoelectric) effect, and the Joule heating on the temperature distribution. The electric field was also modelled in order to come out with the current and voltage distributions. The governing equations were discretized by means of the finite-volume method, whereas the TDMA algorithm was adopted for solving the sets of linear equations. An explicit solution scheme was employed to address the temperature influence on the thermoelectric effect. The model results have been compared with experimental data, when a satisfactory agreement was achieved for both cooling capacity and COP, with errors within a 10% band. In addition, the model was employed to assess the effects of the thermophysical properties and the couple geometry on the thermodynamic performance of the thermoelectric cell.

1. Introduction

In the past decades, solid-state cooling technologies have come onto some particular market niches, especially the applications related to portable cooling [1]. The most significant advances have been achieved in the realm of thermoelectric cooling [2], in which an electric current produces a temperature difference in a couple of dissimilar semiconductor materials. A typical thermoelectric module is manufactured with two thin ceramic wafers and an array of p- and n-type blocks of doped semiconductor material sandwiched between them. A pair of p- and n-type blocks connected electrically in series and thermally in parallel make up a thermoelectric couple [3].

Several studies have been conducted both theoretically and numerically to assess the thermodynamic performance of thermoelectric cells. Samples of the most influencing works are summarised in Table 1. The literature review points out that most models are one-dimensional, being not able to evaluate the influence of the cell geometry on its performance. In addition, the literature analysis also reveals that the few available multidimensional approaches are often developed aided by commercial packages, which provide restricted access to the mathematical formulation and the numeric algorithm. At last, most models do not account for the heat transfer in the air cavity, which may also affect the system performance. The present paper is therefore aimed at advancing a tailor-made two-dimensional model, in the realm of the irreversible thermodynamics, which is suitable to evaluate the sensitivity of the thermophysical properties and the cell geometry on its thermodynamic performance.

☆ An abridged version of this manuscript has been accepted to be presented at the 15th International Refrigeration and Air Conditioning Conference at Purdue, July 14–17, 2014.

* Corresponding author. Tel./fax: +55 41 3361 3239.
E-mail address: chermes@ufpr.br (C.J.L. Hermes).

http://dx.doi.org/10.1016/j.apenergy.2014.05.050
0306-2619/

Nomenclature

Roman

COP	coefficient of performance (W W^{-1})
j	electric current density (A m^{-2})
k	thermal conductivity (W m^{-1} K^{-1})
L_x	width (m)
L_y	height (m)
L_z	length (m)
m	number of control volumes (y-direction)
n	number of control volumes (x-direction)
N	number of thermoelectric couples in the cell
Nu	Nusselt number (dimensionless)
$\dot{q}$	volumetric heat generation rate (W m^{-3})
q	heat flux (W m^{-2})
$\dot{Q}$	heat transfer rate (W)
T	temperature (K)
V	voltage (V)
Z	figure-of-merit (K^{-1})

Greek

α	Seebeck coefficient (V K^{-1})
γ	electrical conductivity (A V^{-1} m^{-1})
φ	generic variable
ρ	electrical resistivity (Vm A^{-1})
τ	Thomson coefficient (V K^{-1})
$\dot{\Psi}$	dimensionless response variable
λ	coefficients of Eq. (27)
$\dot{\varphi}$	dimensionless values of φ

Subscripts

c	cold end
e, w, n, s	control surfaces
P, E, W, N, S	control volumes
h	hot end

2. Mathematical model

A thermoelectric cell is comprised of several couples of p and n semiconductors connected electrically in series and thermally in parallel, and separated from each other by a cavity filled with air. In the present work, the physical model is restricted to a thermoelectric couple, as illustrated in Fig. 1, which in turn is subdivided into ten domains, as summarised in Table 2. The dimensions in Table 2 refer to the thermoelectric device under analysis [13], which has been taken as reference for the present study given its application to portable coolers [14].

The mathematical model is based on the following key assumptions: (i) steady-state two-dimensional approach, (ii) thermoelectric properties regarded as functions of the temperature only, (iii) negligible internal contact resistances (both thermal and electric), (iv) both n and p elements have the same Seebeck coefficient, but with different signs, and (v) heat transfer by both advection and radiation are disregarded, so that $Nu = 1$ in the cavity. Thus, a local energy balance yields,

$$\vec{\nabla} \cdot \vec{q} = \dot{q} \tag{1}$$

where $\dot{q}$ is the rate of heat generation, and the heat flux, $\vec{q}$, is calculated from the following fundamental relation obtained from the irreversible thermodynamics [15]:

$$\vec{q} = -k\vec{\nabla}T + \alpha T\vec{j} \tag{2}$$

where first term on the right-hand side stands for the heat conduction (referred hereafter as Fourier effect), where k is the thermal conductivity, and the second term is associated with the

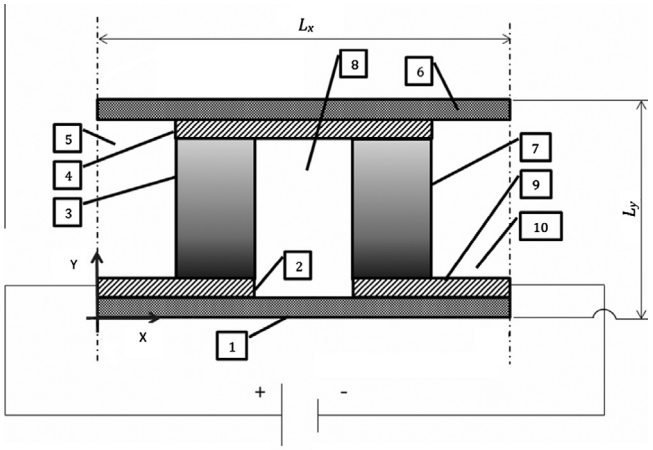

Fig. 1. Schematic representation of the physical model.

Seebeck effect, where α is the Seebeck coefficient. The divergent of Eq. (2) yields,

$$\vec{\nabla} \cdot \vec{q} = -\vec{\nabla} \cdot \left(k\vec{\nabla}T\right) + T\vec{j} \cdot \vec{\nabla}\alpha + \alpha\vec{j} \cdot \vec{\nabla}T + \alpha T\left(\vec{\nabla} \cdot \vec{j}\right) \tag{3}$$

where $\vec{\nabla} \cdot \vec{j} = 0$ at steady-state conditions to ensure the continuity of the current density. In addition, the definition of electric field yields,

$$-\vec{\nabla}V = \rho\vec{j} + \alpha\vec{\nabla}T \tag{4}$$

Table 1
Recent literature on performance assessment of thermoelectric cells.

Author	Year	Approach	Thomson effect	Cavity convection	Cavity radiation	Physical domain	Properties as $f = f(T)$
Huang et al. [4]	2005	Analytical	Yes	Yes	Yes	1D	No
Pramanick and Das [5]	2006	Analytical	Yes	No	No	1D	No
Lee and Kim [6]	2006	Numerical	No	No	No	1D	No
Yamashita [7]	2009	Analytical–experimental	Yes	No	No	1D	Yes
Chen et al. [8]	2011	Numerical	Yes	Yes	Yes	3D	No
Meng et al. [9]	2011	Numerical	Yes	Yes	Yes	1D	Yes
Du and Wen [10]	2011	Numerical–experimental	Yes	No	No	1D	Seebeck only
Chen et al. [11]	2012	Numerical	Yes	No	No	3D	Seebeck only
Pérez-Aparicio et al. [12]	2012	Numerical	Yes	Yes	Yes	3D	Yes

Table 2
Summary of the physical subdomains and thermophysical properties.

Subdomain	Description	Material	Dimensions (mm)	k (W/mK)	γ (V/Am)
1 and 6	Bottom (1) and top (6) electric insulators	Al_2O_3	4.8 × 0.62	30	–
2 and 9	Left (2) and right (9) electric conductors at the bottom	Cu	1.9 × 0.41	400	5.96×10^7
3 and 7	n-type (3) and p-type (7) semiconductors	Bi_2Te_3	1.4 × 1.14	Eq. (12)	Eq. (11)
4	Electric conductor at the top	Cu	1.9 × 0.41	400	5.96×10^7
5 and 10	Left (5) and right (10) side air cavities	Air	0.5 × 1.55	0.026	–
8	Central air cavity	Air	1.0 × 1.55	0.026	–

Therefore, the rate of heat generation $\dot{q}$ can be calculated from:

$$\dot{q} = \vec{j}\cdot\left(-\vec{\nabla}V\right) = \rho\left(\vec{j}\cdot\vec{j}\right) + \alpha\vec{j}\cdot\vec{\nabla}T \tag{5}$$

where the first term on the right-hand side stands for the Joule heating, whereas the second term is regarded with the work produced by the electric current against the Seebeck effect. Invoking the following thermoelectric relation [15],

$$\tau\, dT = T\, d\alpha \tag{6}$$

and substituting Eqs. (3) and (5) into Eq. (1), the following equation for the temperature distribution in a thermoelectric material can be derived,

$$\vec{\nabla}\cdot\left(k\vec{\nabla}T\right) - \tau\vec{j}\cdot\vec{\nabla}T + \rho\left(\vec{j}\cdot\vec{j}\right) = 0 \tag{7}$$

where the first term refers to the Fourier (heat) conduction, the second one to the Thomson (thermoelectric) effect, and the third one to the Joule heating. Writing Eq. (4) for the electric current, recalling that $\vec{\nabla}\cdot\vec{j} = 0$ at steady-state conditions, one can derive the following expression for the voltage distribution along the domain,

$$\vec{\nabla}\cdot\left(\gamma\vec{\nabla}V\right) + \vec{\nabla}\cdot\left(\gamma\alpha\vec{\nabla}T\right) = 0 \tag{8}$$

where $\gamma = 1/\rho$ is the electrical conductivity. The first term stands for the electric conduction, whereas the second one refers to the distortion on the electric field induced by the thermoelectric effect. Eqs. (7) and (8) rule the thermoelectric phenomena, being both expressed for 2-D Cartesian domain as follows:

$$\frac{\partial}{\partial x}\left(k\frac{\partial T}{\partial x}\right) + \frac{\partial}{\partial y}\left(k\frac{\partial T}{\partial y}\right) - \tau\left(j_x\frac{\partial T}{\partial x} + j_y\frac{\partial T}{\partial y}\right) + \rho\left(j_x^2 + j_y^2\right) = 0 \tag{9}$$

$$\frac{\partial}{\partial x}\left(\gamma\frac{\partial V}{\partial x}\right) + \frac{\partial}{\partial y}\left(\gamma\frac{\partial V}{\partial y}\right) + \frac{\partial}{\partial x}\left(\gamma\alpha\frac{\partial T}{\partial x}\right) + \frac{\partial}{\partial y}\left(\gamma\alpha\frac{\partial T}{\partial y}\right) = 0 \tag{10}$$

where j_x and j_y are the x and y components of the current density, respectively, in (A/m^2). Eqs. (9) and (10) require two boundary conditions each. For the latter, prescribed inlet (V_{in}) and outlet (V_{out}) voltages were adopted. In addition, bearing in mind that there is no electron flux through subdomains 1 and 6, $dV/dy = 0$ boundary conditions have also been adopted. In case of Eq. (9), prescribed temperatures were used for both hot (T_h) and cold ($T_c = T_h - \Delta T$) ends. Zero heat flux boundary conditions ($dT/dx = 0$) were additionally employed for the cell symmetry. Fig. 2 depicts the conditions used for each boundary of the physical domain. The thermophysical properties of the Bi_2Te_3-elements were calculated from 2nd-order polynomial fits obtained from data provided by Rowe [16],

$$\rho = 2.3935\times10^{-11}T^2 + 2.9771\times10^{-8}T - 8.959\times10^{7} \tag{11}$$

$$k = 3.682\times10^{-5}T^2 - 2.372\times10^{-2}T + 5.388 \tag{12}$$

$$\alpha = -8.5952\times10^{-10}T^2 + 8.0546\times10^{-7}T + 4.329\times10^{-5} \tag{13}$$

where T is in (K), ρ in (Vm/A), k in (W/mK), and α in (V/K). The Thomson coefficient, τ, was calculated from Eqs. (6) and (13). Both the air and the Al_2O_3-elements were assumed to be perfect electric insulators, with thermal conductivities (at 300 K) of 30 and 0.026 W/mK, respectively. For the copper, a thermal conductivity of 400 W/mK and an electrical conductivity of 5.96×10^7 A/Vm have been adopted. The heat transfer inside the air cavity has been modelled assuming a unitary Nusselt number, so that the effects of free convection and radiation have been neglected.

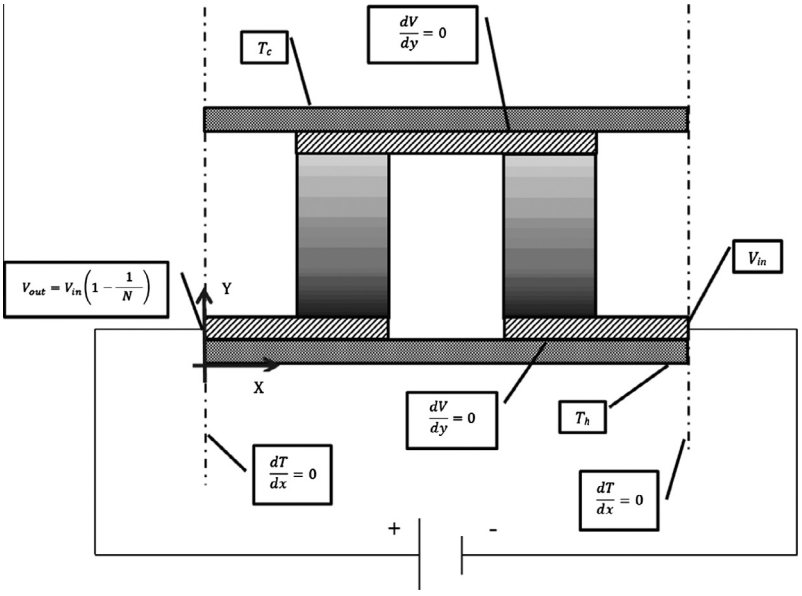

Fig. 2. Physical domain with boundary conditions.

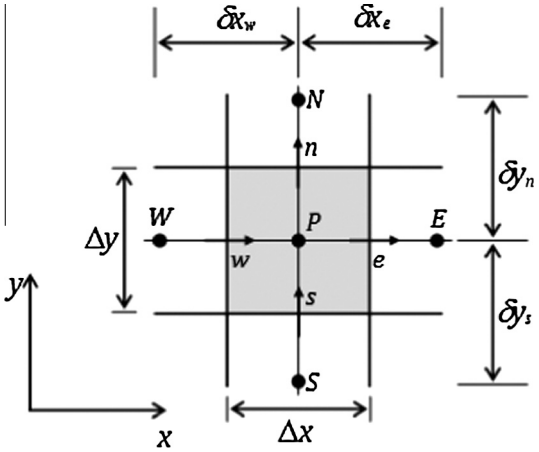

Fig. 3. Typical control volume of the discretized domain.

3. Numerical scheme

Because of the non-linearities, Eqs. (9) and (10) must be solved iteratively in order to come out with the temperature and voltage distributions along the domain. The computational code was written in-house based on the so-called finite-volume method [17] to provide access to the numerical schemes in the present and also in further researches. The method consists of dividing the physical domain into non-overlapping control volumes in which the transported quantities are conserved. The centroid of each control volume, as illustrated in Fig. 3, corresponds to an integration point of the discretized domain. The properties (T, V) are evaluated at the centroids, whereas the fluxes (q, j) are evaluated at the control surfaces. A non-uniform Cartesian mesh was generated by means of the equation introduced by Wood [18]. Mesh independent solutions have been found for computational grids with 3000+ control volumes. A snapshot of a computational domain with 3120 control volumes is depicted in Fig. 4.

Eqs. (9) and (10) were discretized using a 2nd-order central-differencing scheme. The non-linear terms have been incorporated into the source term. The resulting algebraic equations for temperature and voltage are as follows:

$$A_P^T T_P = A_e^T T_E + A_w^T T_W + A_n^T T_N + A_s^T T_s + B^T$$

$$\begin{cases} A_e^T = k_e \Delta y/\delta x_e \\ A_w^T = k_w \Delta y/\delta x_w \\ A_n^T = k_n \Delta x/\delta y_n \\ A_s^T = k_s \Delta x/\delta y_s \\ A_P^T = A_e^T + A_w^T + A_n^T + A_s^T \\ B^T = \rho_P\left(j_x^2 + j_y^2\right)\Delta x \Delta y - \tau_P\left(j_x\left(T_e^* - T_w^*\right)\Delta y + j_y\left(T_n^* - T_s^*\right)\Delta x\right) \end{cases} \tag{14}$$

$$A_P^V V_P = A_e^V V_E + A_w^V V_W + A_n^V V_N + A_s^V V_s + B^V$$

$$\begin{cases} A_e^V = \gamma_e \Delta y/\delta x_e \\ A_w^V = \gamma_w \Delta y/\delta x_w \\ A_n^V = \gamma_n \Delta x/\delta y_n \\ A_s^V = \gamma_s \Delta x/\delta y_s \\ A_P^V = A_e^V + A_w^V + A_n^V + A_s^V \\ B^V = \alpha_e A_e^V T_E^* + \alpha_w A_w^V T_W^* + \alpha_n A_n^V T_N^* + \alpha_s A_s^V T_S^* \\ \qquad -\left(\alpha_e A_e^V + \alpha_w A_w^V + \alpha_n A_n^V + \alpha_s A_s^V\right) T_P^* \end{cases} \tag{15}$$

where the superscripted asterisk stands for the property evaluated from the previous iteration. The components of the electron flux at the control surfaces n, s, e, and w are calculated as follows:

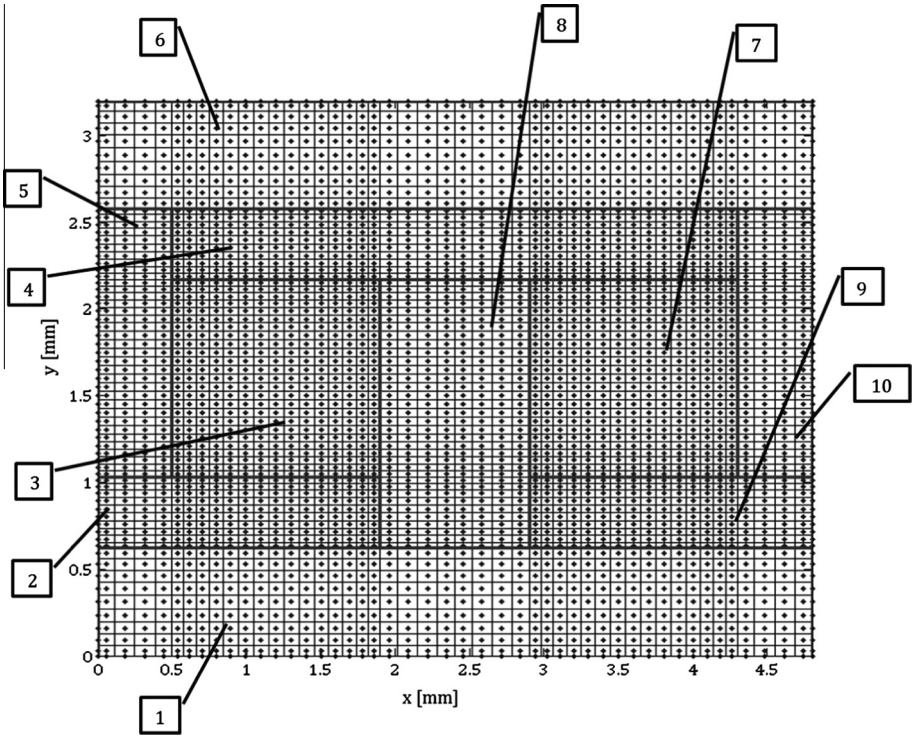

Fig. 4. Non-uniform grid with 3120 control volumes (see Table 2 for the summary of the physical subdomains).

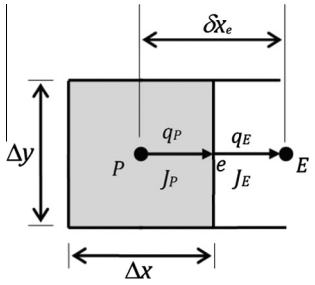

Fig. 5. Continuity of heat and current fluxes at the interface.

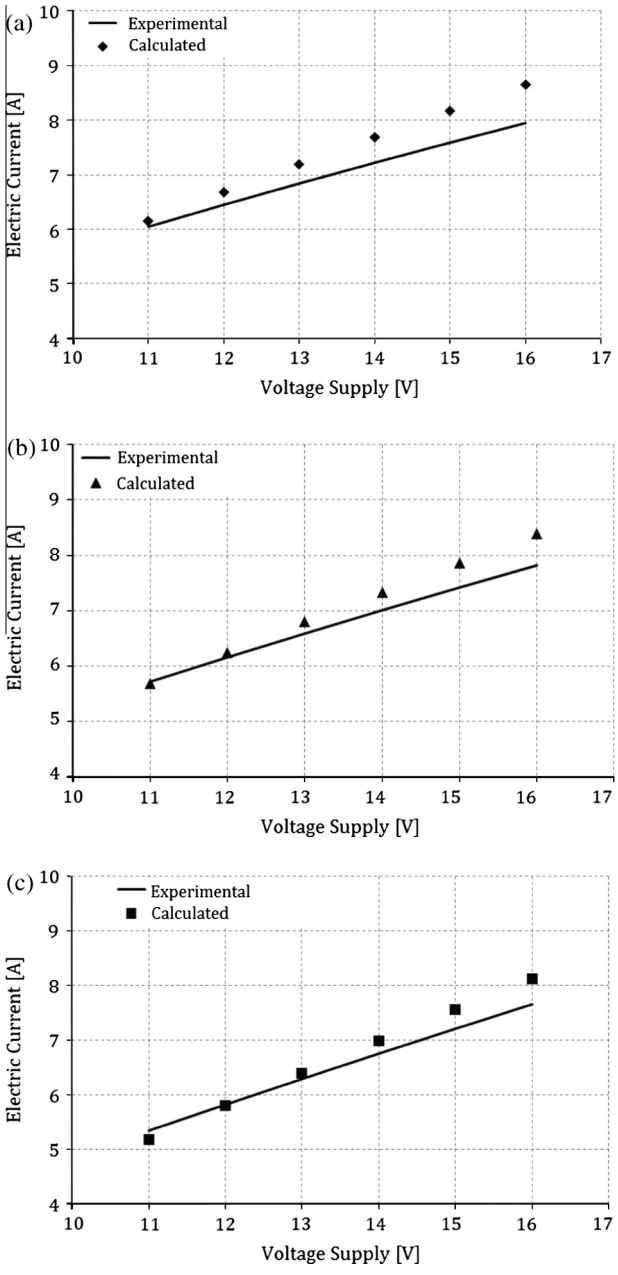

Fig. 6. Comparison between calculated and experimental electric current: (a) $\Delta T = 0$ K, (b) $\Delta T = 30$ K and (c) $\Delta T = 60$ K.

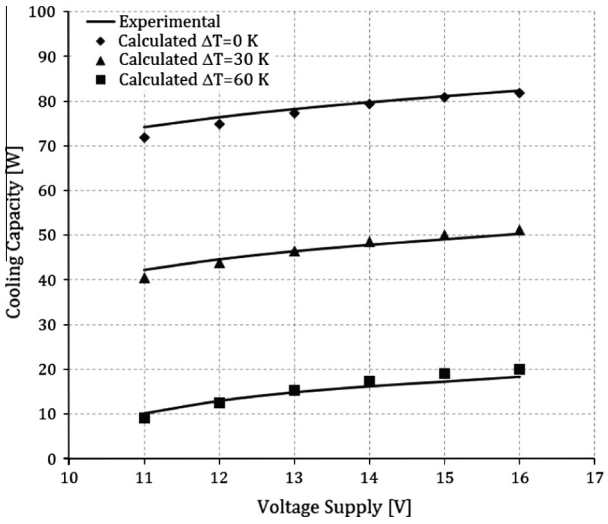

Fig. 7. Comparison between calculated and experimental cooling capacity.

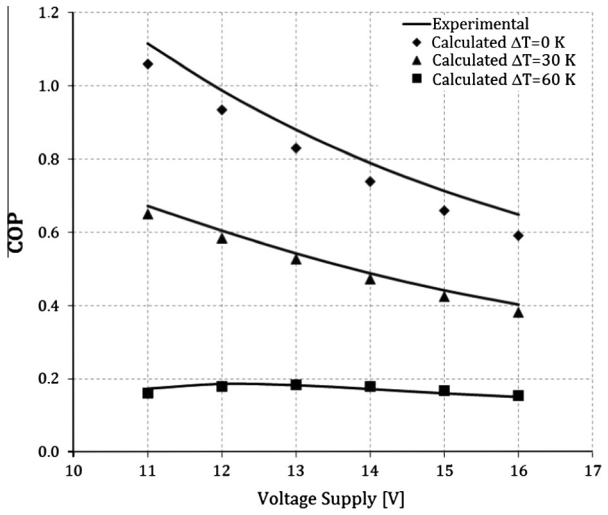

Fig. 8. Comparison between calculated and experimental COP.

$$j_n = -\frac{\gamma_n}{\delta y_n}[(V_N - V_P) + \alpha_n(T_N - T_P)] \tag{16}$$

$$j_s = -\frac{\gamma_s}{\delta y_s}[(V_P - V_S) + \alpha_s(T_P - T_S)] \tag{17}$$

$$j_e = -\frac{\gamma_e}{\delta y_e}[(V_E - V_P) + \alpha_e(T_E - T_P)] \tag{18}$$

$$j_w = -\frac{\gamma_w}{\delta y_w}[(V_P - V_W) + \alpha_w(T_P - T_W)] \tag{19}$$

Therefore, the x and y components of the electron flux are calculated from:

$$j_x = \frac{j_e \delta x_e + j_w \delta x_w}{\delta x_e + \delta x_w} \tag{20}$$

$$j_y = \frac{j_n \delta y_n + j_s \delta y_s}{\delta y_n + \delta y_s} \tag{21}$$

The temperature and voltage at the interfaces between different materials are calculated in order to guarantee the continuity of the electric current and heat fluxes (see Fig. 5) as follows:

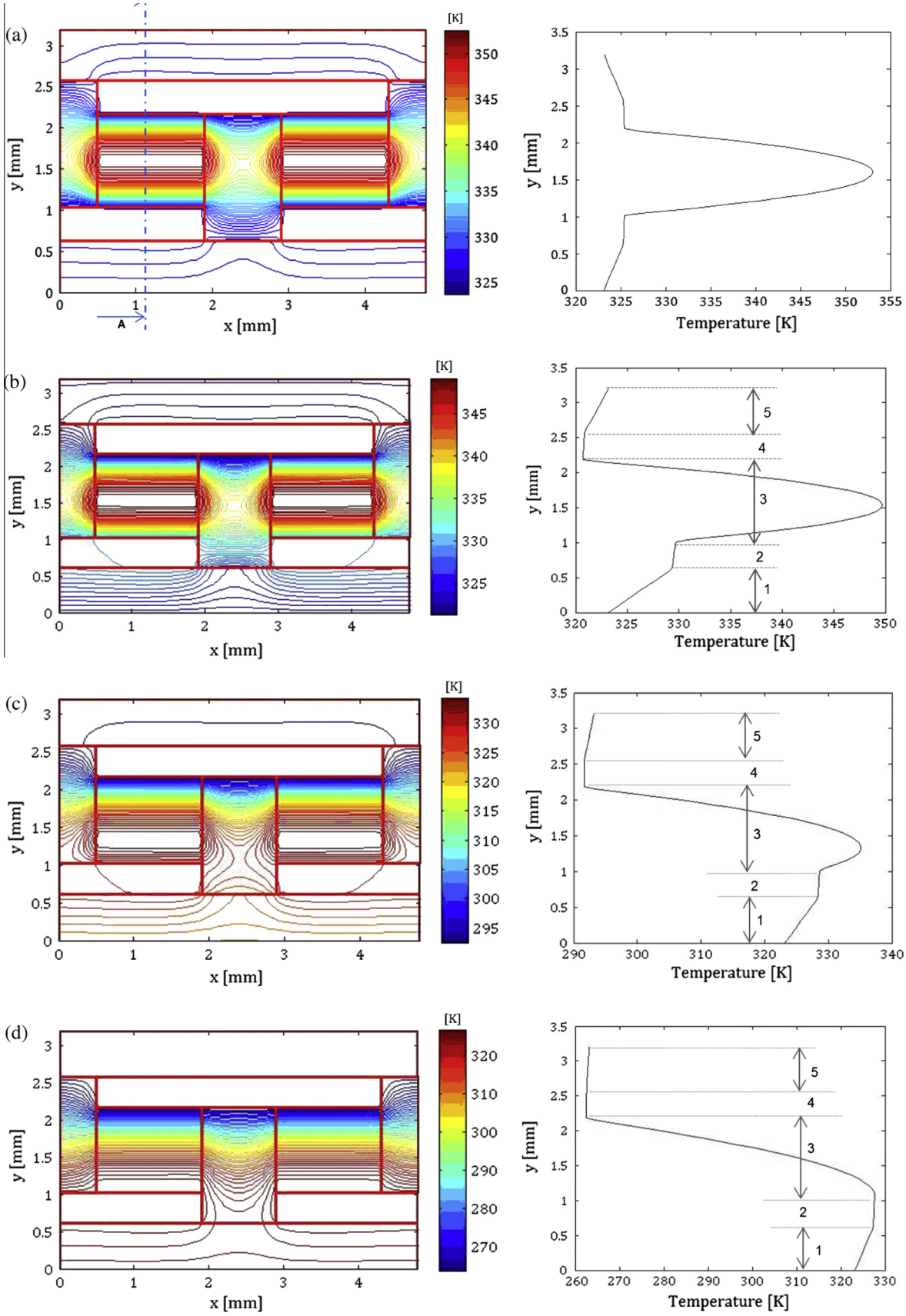

Fig. 9. Temperature distribution along the domain for $\Delta V = 16$ V and different ΔT (1 and 5 – Al_2O_3 wafer, 2 and 4 – Cu contacts , and 3 – thermoelectric element).

$$T_e = (1-f_e)T_P + f_e T_E + \frac{(\alpha T j)_E - (\alpha T j)_P}{\frac{2k_P}{\Delta x_P} + \frac{2k_E}{\Delta x_E}} \quad (22)$$

$$V_e = (1-f_e)V_P + f_e V_E + \frac{\alpha_E(T_P - T_e) - \alpha_P(T_e - T_P)}{\frac{2\gamma_P}{\Delta x_P} + \frac{2\gamma_E}{\Delta x_E}} \quad (23)$$

where $f_e = \frac{1}{2}\Delta x_E/\delta x_e$. The sets of linear equations have been solved iteratively through the so-called tri-diagonal matrix algorithm (TDMA). In addition to the boundary conditions, the input variables are the thermophysical properties of the composing materials, and the cell dimensions, all described in Table 2. More detailed information on the numerical scheme can be found in [19].

4. Results and discussion

4.1. Model validation

The code predictions were validated against experimental data obtained from the manufacturer of a particular thermoelectric module [13]. All simulations were carried out for $T_h = 323$ K, but varying the ΔT between the hot and the cold ends from 0 to 60 K, and the ΔV applied to the whole thermoelectric cell. Fig. 6 shows a comparison between the calculated and measured electric current, where one can see the maximum difference achieved (for $\Delta T = 0$ K and $\Delta V = 16$ V) was below the 10% threshold, while the average difference lies around 4%. In all cases, it can be seen the model is able to reproduce the experimental trends satisfactorily. One should also note that Fig. 6 illustrates the behaviour described by Eq. (4), where a decreasing ΔT leads to a current increase for a given ΔV because of the Seebeck effect.

Additional validation parameters are the cooling capacity $\dot{Q}_c$ and the COP, calculated respectively as follows:

$$\dot{Q}_c = NL_z \sum_{i=1}^{n} \left(k \frac{T_m - T_c}{\delta y_m} \Delta x \right)_i \quad (24)$$

$$\mathrm{COP} = \frac{\dot{Q}_c}{\dot{Q}_h - \dot{Q}_c} \quad (25)$$

where $\dot{Q}_h$ is the heat released at the hot end, calculated as follows:

$$\dot{Q}_h = NL_z \sum_{i=1}^{n} \left(k \frac{T_h - T_1}{\delta y_1} \Delta x \right)_i \quad (26)$$

where L_z is the cell dimension in the z-direction (perpendicular to the paper sheet), N is the number of thermoelectric couples in the cell, and n and m are the number of control volumes in the x and y directions, respectively. Fig. 7 shows the calculated and the experimental cooling capacities agreed to with errors within the 10% threshold. The higher difference is observed for low voltages and $\Delta T = 0$ K. A similar behaviour is observed in Fig. 8 for the COP. In all cases, the experimental trends are well reproduced by the model.

4.2. Temperature distribution

Fig. 9 explores the temperature distributions obtained for four different cases: (a) no thermoelectric effect (Joule heating only) and $\Delta T = 0$ K; (b) thermoelectric effect and $\Delta T = 0$ K; (c) thermoelectric effect and $\Delta T = 30$ K; and (d) thermoelectric effect and $\Delta T = 60$ K. In all cases, $\Delta V = 16$ V. The temperature profiles along the A-A cut (at $x = 1.1$ mm) are also depicted in Fig. 9. For case (a), where no thermoelectric effect takes place, one can see that the Joule heating is symmetrically dissipated by Fourier conduction in such a way the maximum temperature takes place at the centre of the thermoelectric elements. This is so as $\Delta T = 0$ K. In cases the thermoelectric effect is on, the locus of the maximum temperature migrates from the centre to the bottom inasmuch ΔT increases.

4.3. Thermoelectric properties

The sensitivity analysis was carried out considering as response variables the cooling capacity and the COP, whereas the thermophysical properties (i.e. thermal conductivity, Seebeck coefficient, and electric conductivity) have been taken as independent parameters. A 2-level, 3-factor factorial design was then structured totalizing 8 runs. The levels span ±5% taking the figures provided by Eqs. (11)–(13) as reference. The simulation runs were carried out for $\Delta T = 0$ K and $\Delta V = 16$ V. The regression model adopted in this work is as follows:

$$\hat{\Psi} = \lambda_0 + \lambda_1\hat{k} + \lambda_2\hat{\alpha} + \lambda_3\hat{\gamma} + \lambda_4\hat{k}\hat{\alpha} + \lambda_5\hat{k}\hat{\gamma} + \lambda_6\hat{\alpha}\hat{\gamma} + \lambda_7\hat{k}\hat{\alpha}\hat{\gamma} \quad (27)$$

where $\gamma = 1/\rho$ is the electric conductivity, $\hat{\Psi}$ is the dimensionless response variable, λ are the coefficients calculated from the least-squares method, and $\hat{\varphi}$ are the dimensionless values of φ, calculated from:

$$\hat{\varphi} = 2\frac{\varphi - \varphi_{\min}}{\varphi_{\max} - \varphi_{\min}} - 1 \quad (28)$$

Fig. 10 shows the cooling capacity is mainly affected by the electric conductivity and the Seebeck coefficient, and marginally affected by the thermal conductivity, which play a negative role on the cooling capacity. Higher order interactions have not played any material roles on the cooling capacity. Fig. 10 also shows the effects of the thermophysical properties on the COP, where one can see the Seebeck coefficient plays a dominant role, followed by the thermal and electric conductivities, which played marginal effects. These results are confirmed by the definition of the figure-of-merit of the thermoelectric material, $Z = \alpha^2\gamma/k$, which is straightforwardly related to the COP [15].

4.4. Aspect ratio

To assess the influence of the geometry, the aspect ratio was varied by increasing the height of the thermoelectric cell, L_y, in two fashions: (a) constrained base area (i.e. fixed L_x, see Fig. 11a), and (b) constrained volume of thermoelectric material (see Fig. 11b). In all cases, $\Delta T = 0$ K and the voltage was varied from 14 to 20 V. Fig. 12 shows the COP is weakly affected by L_y. Actually, a slight increase can be observed. This is so as the cooling capacity depletes inasmuch the electric current decreases, which diminishes the power consumption at the same rate. As the COP stands for the ratio between the cooling capacity and the power consumption, one may expect the COP-value does not change significantly from one case to the other.

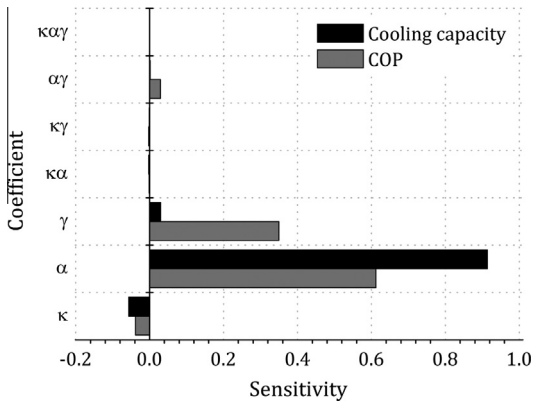

Fig. 10. Results of the sensitivity analysis: cooling capacity and COP.

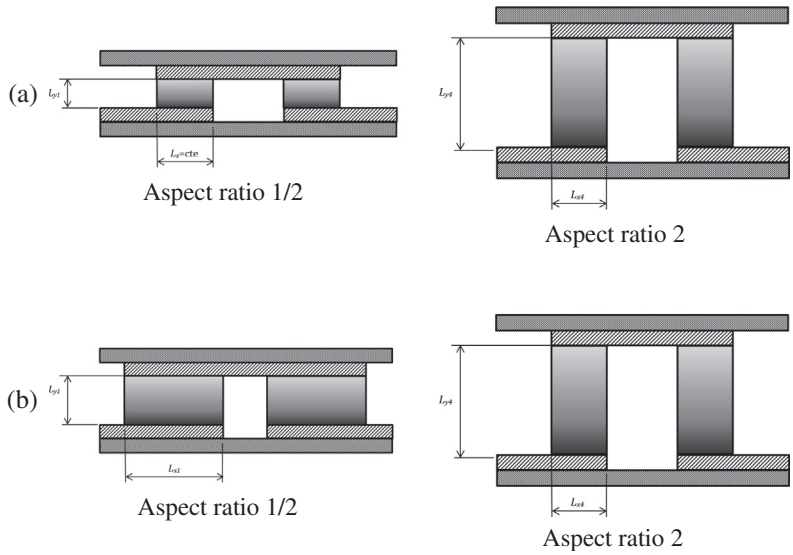

Fig. 11. Samples of geometries analysed in case of (a) constrained base area, and (b) constrained volume.

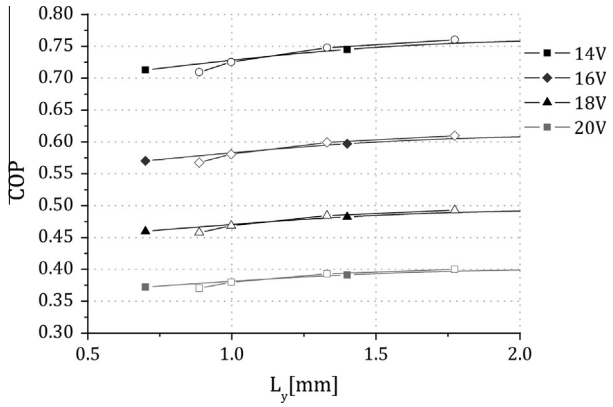

Fig. 12. Influence of the aspect ratio on the COP in case of constrained area (solid bullets) and constrained volume (open bullets).

5. Summary and conclusions

A two-dimensional steady-state model was put forward to evaluate the thermodynamic performance of thermoelectric cells in the realm of the irreversible thermodynamics. The model takes into account the Fourier conduction, the Joule heating, and the Thomson effect, being able to predict the cooling capacity, the power consumption, and the COP in case of prescribed voltage supply, and prescribed temperatures at the hot and cold ends. The governing equations were discretized by means of the finite-volume method using a central-differencing scheme. The non-linearities typical of the thermoelectric phenomena were embedded into the source term, and the resulting sets of algebraic equations were solved iteratively by the TDMA algorithm.

The tailor-made model was coded in-house and its predictions for electric current, cooling capacity and COP were compared against experimental data obtained from the manufacturer of a particular thermoelectric cell. It was observed that the numerical predictions and experimental data not only agreed to within 8.8% thresholds (electric current), 10% thresholds (cooling capacity), and 7.3% thresholds (COP), but also that the model is able to follow the experimental trends very closely. The model can be used either to access the performance of an existing cell for given working conditions (ΔT, ΔV or current) or to design a new one (geometry, selection of materials) subjected to working constraints (cooling capacity, COP).

The influence of the thermophysical properties on the response variables (cooling capacity and COP) was assessed by means of a 2^3 factorial design, which has pointed out that the Seebeck coefficient and the thermal conductivity play major roles on the cooling capacity, whereas the COP is more sensible to the Seebeck coefficient. The influence of the geometry was also assessed by varying the aspect ratio according to two different ways: constrained base area and constrained volume. It was found that both the cooling capacity and the power consumption vary at the same rate, in such a way the COP has showed a comparable behaviour for constrained base area and constrained volume of thermoelectric material.

Acknowledgements

This study was carried out under the auspices of the Brazilian funding agencies CAPES and CNPq.

References

[1] Hermes CJL, Barbosa JR. Thermodynamic comparison of Peltier, Stirling, and vapor compression portable coolers. Appl Energy 2012;91:51–8.
[2] Riffat SB, Ma X. Thermoelectrics: a review of present and potential applications. Appl Therm Eng 2003;23:913–35.
[3] Tassou SA, Lewis JS, Ge YT, Hadawey A, Chaer I. A review of emerging technologies for food refrigeration applications. Appl Therm Eng 2010; 30:263–76.
[4] Huang M, Yen R, Wang A. The influence of the Thomson effect on the performance of a thermoelectric cooler. Int J Heat Mass Transfer 2005;48: 413–8.
[5] Pramanick AK, Das PK. Constructal design of a thermoelectric device. Int J Heat Mass Transf 2006;49:1420–9.
[6] Lee KH, Kim OJ. Analysis on the cooling performance of the thermoelectric micro-cooler. Int J Heat Mass Transf 2006;50:1892–992.
[7] Yamashita O. Effect of linear and non-linear components in the temperature dependences of thermoelectric properties on the cooling performance. Appl Energy 2009;86:1746–56.
[8] Chen M, Rosendahl LA, Condra T. A three-dimensional numerical model of thermoelectric generators in fluid power systems. Int J Heat Mass Transf 2011; 54:345–55.
[9] Meng F, Chen L, Sun F. A numerical model and comparative investigation of a thermoelectric generator with multi-irreversibilities. Energy 2011;36: 3513–22.
[10] Du C, Wen C. Experimental investigation and numerical analysis for one-stage thermoelectric cooler considering Thomson effect. Int J Heat Mass Transf 2011;54:4875–84.

[11] Chen W, Liao C, Hung C. A numerical study on the performance of miniature thermoelectric cooler affected by Thomson effect. Appl Energy 2012;89:464–73.
[12] Pérez-Aparicio JL, Palma R, Taylor RL. Finite element analysis and material sensitivity of Peltier thermoelectric cells coolers. Int J Heat Mass Transf 2012;55:1363–74.
[13] Tellurex. Module Specification – Z-max – C1-1.4-127-1.14. Traverse City-MI, USA; 2007.
[14] Duarte, POO. Performance evaluation of a thermoelectric refrigerator (in Portuguese). M.Eng. thesis, Federal University of Santa Catarina, Florianopolis-SC, Brazil; 2003. 114p.
[15] Reynolds WC. Thermodynamics. McGraw-Hill; 1968. 496p.
[16] Rowe D. CRC handbook of thermoelectrics. CRC Press; 1995.
[17] Patankar SV. Numerical heat transfer and fluid flow. Hemisphere Publishing Co.; 1980.
[18] Wood WA. Multigrid approach to incompressible viscous cavity flow. Hampton (VA, USA): Technical Memorandum, NASA Langley Research Center; 1996.
[19] Oliveira KMS. Numerical assessment of the thermodynamic behavior of thermoelectric cells (in Portuguese). M.Eng. thesis, Federal University of Paraná, Curitiba-PR, Brazil; 2014. 140p.